Solar Energy Materials & Solar Cells 155 (2016) 243–252

Contents lists available at ScienceDirect

Solar Energy Materials & Solar Cells

journal homepage: www.elsevier.com/locate/solmat

Solution-processed pH-neutral conjugated polyelectrolytes with one-atom variation (O, S, Se) as a novel hole-collecting layer in organic photovoltaics

Min-Hee Choi, Eui Jin Lee, Jae Pil Han, Doo Kyung Moon *

Department of Materials Chemistry and Engineering, Konkuk University, 1 Hwayang-dong, Gwangjin-gu, Seoul 143-701, South Korea

ARTICLE INFO

Article history:
Received 7 March 2016
Received in revised form
7 June 2016
Accepted 12 June 2016
Available online 18 June 2016

Keywords:
Conjugated polyelectrolytes
pH-neutral hole transporting layer
Heterocyclic ring
Dipole moment
Surface potential difference
Bulk heterojunction polymer solar cell

ABSTRACT

We present pH-neutral hole transporting layers processed from a solution at room temperature for organic photovoltaics (OPVs). Three new conductive conjugated polyelectrolytes (CPEs), identified as PFF, PFT and PFSe, containing aromatic five-membered heterocyclic compounds (furan, thiophene, and selenophene, respectively), are designed and synthesized using the Stille-coupling reaction. These polymers dissolve in water/alcohol as they are comprised of a conjugated backbone with hydrophilic side chains of sodium butane sulfonates. The CPEs with heterocyclic rings having stronger dipole moments decrease the work function of ITO electrodes and the surface potential between the active layer and hole-transporting layer (HTL) effectively. The device with PFSe as a HTL exhibits the best performance (7.2%), with J_{SC} of 14.4 mAcm^{-2}, V_{OC} of 0.677 V and FF of 69.0%. The device also exhibits improvements in air stability under room temperature due to its neutral nature. Also, 70% of its initial power conversion efficiency (PCE) is maintained upon exposure to ambient air for ~480 h, whereas the initial PCE with PEDOT:PSS decreases by more than 50%. Our results indicate that it is possible to improve the performance of OPVs using pH-neutral CPEs as efficient HTLs. We determine the way of molecular design is used to decrease the energy barrier using a heteroatom with a large dipole moment.

1. Introduction

Recently, polymer solar cells (PSCs) have received substantial attention as promising alternatives to inorganic photovoltaic devices in academic research and industrial applications because they are lightweight, flexible, require inexpensive manufacturing and have the possibility of large-scale production via solution processing [1–3]. Molecular design is essential for the development of high performance optoelectronic materials in applications of PSCs. Extensive research has been devoted to achieving the optimal configuration of the chemical and structural parameters, such as conjugated backbones, side chains and substituents [4–8]. After extensive structural optimization, compounds of the PTB family, such as poly({4,8-bis[(2-ethylhexyl)oxy]benzo[1,2-b:4,5-b′] dithiophene-2,6-diyl}{3-fluoro-2-[(2-ethylhexyl)carbonyl]thieno [3, 4-b]thiophenediyl}) (PTB7), exhibited excellent photovoltaic performance. A power conversion efficiency (PCE) of approximately 7.4% has been achieved using PTB7/[6,6]-phenyl C71 butyric acid methyl ester ($PC_{71}BM$) conventional solar cell devices [9]. Furthermore, inverted PSCs have led to PCEs higher than 8.2% [10]. In addition to designing new active materials to enhance the PCE and device stability, morphology optimization and interface engineering of bulk heterojunction (BHJ) solar cells are also fundamentally important [11–14].

To improve the charge selectivity at the electrodes and to minimize the energy barrier for charge extraction, a hole-transporting layer (HTL) with electron-blocking properties is inserted between the anode and the BHJ active layer. Moreover, an electron-transporting layer (ETL) with hole-blocking properties is inserted between the cathode and BHJ active layer [15–17]. The polymer poly (3,4-ethylenedioxythiophene):poly(styrenesulfonate) (PEDOT:PSS) is the most widely employed as a HTL material for PSCs, because of its solution processability, appropriate work function, sufficient conductivity, and high optical transparency in the visible-NIR region. However, PEDOT:PSS is highly acidic, and the strong anisotropy in electrical conduction in spin-coated PEDOT:PSS layers, originating from their lamellar structures, often limits charge collection in solar cells. In solar cells, the active layer has the chemical interaction at the interface between the active layer and the PEDOT:PSS. Specifically, it determines the chemical instability between the active layer and electrodes in the long-term [18–20]. To overcome

* Corresponding author.
E-mail address: dkmoon@konkuk.ac.kr (D.K. Moon).

http://dx.doi.org/10.1016/j.solmat.2016.06.017
0927-0248/

these deficiencies, conjugated polyelectrolytes (CPEs) are used as an interfacial material for organic photovoltaics. CPEs have received increasing attention because of their ability to improve PCE through solution processing. CPEs comprise π-conjugated backbones (hydrophobic) with ionic functional groups (hydrophilic) and are developed as multifunctional materials [21]. In the past, CPE layers have been utilized as ETLs to improve electron extraction toward the cathode. The advantages of using CPEs as ETLs in BHJ solar cells include reduction of series resistance, increase of internal built-in voltage, and modification of the electron extraction properties of a single device. These advantages facilitate the energy-level-matching at the interface that is essential for these devices to achieve high performance [22–24]. Kim et al. reported that one reason for the improvement is that directly depositing CPE on top of the ITO substrate can tune the electrode's work-function (WF) due to the formation of an aligned interfacial dipole assembly at the metal/organic semiconductor interface. This modifies the energy-level alignment and decreases the charge extraction barrier [25]. In contrast, the function of CPEs in affecting the hole injection/extraction has been rarely addressed.

Although such CPEs show great potential for WF tunability in organic electronic applications, their uses have been limited to lowering the WFs of metals. Thus, some research has been devoted to the development of CPEs by varying their polymeric structures, including their conjugated backbone, ionic functionalities, and the functional group in alkyl side chains [15]. These efforts do not suggest an effective way to modulate dipole strength, which is the determining factor for modifying the WFs of CPE-covered metal electrodes. Lee et al. proposed a doping process to create new dipoles in the functional group of the alkyl side chains and to modulate the WFs of adjacent metal electrodes according to their doping concentrations [26]. However, not all repeating units are oxidized during the oxidation process. This demonstrates the low reproducibility of this method due to the lack of control of the doping concentration using the same oxidants.

Five-membered heterocyclic compounds, such as pyrrole, furan, thiophene and selenophene, have different physical properties because of the different heteroatoms present in each one. Compared with benzenoid compounds, non-benzenoid aromatic compounds have large resonance energy and large dipole moments. The delocalization of the heteroatom lone pairs into π-systems can be inferred from the dipole moments of the aromatic heterocycles, for which the heteroatom is at the negative end of the dipole in the saturated compounds [27,28]. Heteroatoms are incorporated into hybridization, and based on using hybridization and shape molecules can be categorized relative to the strength of their molecular dipole moments.

In this study, we report unique water/alcohol-soluble CPEs: poly[9,9-bis(4′-sulfonatobutyl)fluorene-alt-hetero cyclic ring] (PFF, PFT and PFSe). These are utilized instead of acidic PEDOT:PSS as a HTL. We study the effects of the electronic properties at the interface between the anode and the active layer. The interfacial contact changes the device performance of BHJ solar cells based on PTB7 as the electron donor and $PC_{71}BM$ as the acceptor. We control the work function and the surface potential between anode/HTL and the active layer using different heteroatoms. We demonstrate that high-efficiency organic BHJ solar cells with PCEs of up to 7.2% are successfully achieved when the PEDOT:PSS HTL is replaced by a PFSe with simultaneous improvement in the short-circuit current (Jsc) and the fill factor, as well as 19% higher air stability than PEDOT:PSS during 480 h of exposure to ambient air at room temperature.

2. Experimental

2.1. Materials

All starting materials were purchased from Sigma Aldrich and Alfa Aesar and used without further purification. Sodium 4-(2,7-dibromo-9-(4-sulfonatobutyl)-9H-fluoren-9-yl)butyl sulfite (M1) was synthesized following procedures modified from the literature. In both poly({4,8-bis[(2-ethylhexyl)oxy]benzo[1,2-b:4,5-b′]dithiophene-2,6-diyl}{3-fluoro-2-[(2-ethylhexyl)carbonyl]thieno[3, 4-b]thiophenediyl}) (PTB7) and 1-(3-methoxycarbonyl)propyl-1-phenyl-[6,6]-C71 ($PC_{71}BM$), 1-material products were acquired and used. Commercial poly[(9,9-bis(3′-(N,N-dimethylamino)propyl)-2,7-fluorene)-alt-2,7-(9,9-dioctylfluorene)] (PFN) was utilized as the ETL for comparison.

2.2. General polymerizations

Monomer M1 (1.28 g, 2.0 mmol) and M2 (or M3 or M4) (2.0 mmol) were dissolved in 54 mL of DMF. The resulting solution was deoxygenated using nitrogen for 15 min. Then tris(dibenzylideneacetone)dipalladium(0) (Pd_2dba_3) (91.6 mg, 0.1 mmol, 5 mol%) and tri-(o-tolyl)phosphine (0.12 g, 0.4 mmol, 20 mol%) were added to the stirred solution under the protection of N_2. The reaction mixture was then heated up to 100 °C and stirred for 48 h. The viscous solution was then poured into 300 mL of acetone. The precipitate was collected via vacuum filtration and washed using acetone (300 mL × 2). The polymer precipitate was then dissolved in water and purified via dialysis using 12 kD molecular-weight-cut off (MWCO) regenerated cellulose membranes. After dialysis, the water was removed via the low temperature drying method. The water-soluble PFF, PFT, and PFSe were obtained as yellow or orange solids.

2.2.1. Poly[9,9-bis(4′-sulfonatobutyl)fluorene-alt-furan] (PFF)

Yellow solid, 0.60 g (yield = 55%). ^{1}H NMR (400 MHz, D_2O, d): δ 7.78 (m, 2H), 7.58 (m, 2H), 7.32 (m, 2H), 3.53 (t, 2H), 3.45 (t, 2H), 2.83 (m, 2H), 2.50 (m, 2H), 1.64 (m, 6H), 1.56 (m, 2H), 1.38 (m, 2H).

2.2.2. Poly[9,9-bis(4′-sulfonatobutyl)fluorene-alt-thiophene] (PFT)

Yellow solid, 0.65 g (yield = 58%). ^{1}H NMR (400 MHz, D_2O, d): δ 7.78 (m, 2H), 7.66 (m, 2H), 7.14 (m, 2H), 3.51 (t, 2H), 3.45 (t, 2H), 2.83 (m, 4H), 2.52 (m, 4H), 1.62 (m, 6H), 1.36 (m, 2H).

2.2.3. Poly[9,9-bis(4′-sulfonatobutyl)fluorene-alt-selenophene] (PFSe)

Yellow solid, 0.31 g (yield = 25%). ^{1}H NMR (400 MHz, D_2O, d): δ 7.62 (m, 4H), 7.46 (m, 2H), 3.52 (t, 2H), 3.44 (t, 2H), 2.82 (m, 2H), 2.50 (m, 4H), 1.99 (m, 4H), 1.37 (m, 4H), 0.54 (m, 2H).

2.3. Measurements

The ^{1}H NMR (400 MHz) spectra were recorded using a Brüker AMX400 spectrometer in D_2O, and the chemical shifts were recorded in units of ppm, with TMS as the internal standard. All of the GPC analyses were carried out using Buffer pH 9 + 30% MeOH as the eluent and PEG/PEO as the calibration. The TGA measurements were performed using a TG 209 F3 thermogravimetric analyzer. The work function values and ultraviolet photoelectron spectroscopy (UPS) spectra of the PFT, PFtT, and PFbT thin films on ITO electrodes were obtained using a KP 6500 Digital Kelvin probe (McAllister Technical Services, Co.) and a UPS analysis chamber (2×10^{-8} Torr) equipped with an AXIS Ultra DLD (KRATOS, Inc.) hemispherical electron energy analyzer with a He I ($h\nu = 21.2$ eV) source. The samples were stored under high vacuum overnight before the UPS measurements, and a sample bias of −8.86 V was

used for the UPS to determine the WF of the metal. The WF (ϕ_m) is given by $\phi_m = h\nu - W$, where $h\nu$ is the incident UV light, and W is the measured width of the emitted electrons (W) from the onset of the secondary electrons to the Fermi edge. The absorption spectra and transmittance spectra were recorded using an Agilent 8453 UV–visible spectroscopy system. The solutions that were used for the UV–visible spectroscopy measurements were dissolved in MeOH. The current density–voltage (J–V) curves of the photovoltaic devices were measured using a computer-controlled Keithley 2400 source measurement unit (SMU) equipped with a Class A Oriel solar simulator under an illumination of AM 1.5 G (100 mW cm^{-2}). The incident photon-to-current conversion (IPCE) was measured to determine the best device performance using the Mc Science IPCE measurement system with monochromatic light, which uses a xenon lamp (Oriel 96000 150 W solar simulator) to pass light through a monochromator (Oriel Cornerstone 130 1/8 m monochromator). The spectral response was normalized by using a standard mono-silicon solar cell before the IPCE data was taken. Atomic force microscopy (AFM) in tapping mode and electrostatic force microscopy (EFM) were performed using an XE-100 instrument under ambient conditions to obtain topographic images of the HTLs and surface potentials. The surface energy was measured using a contact angle meter (KRUSS K6).

2.4. Photovoltaic cell fabrication and treatment

All the bulk-heterojunction PV cells with the ITO/HTL/PTB7:$PC_{71}BM$/PFN/Al device architecture were prepared according to the following fabrication procedure. The glass/indium tin oxide (ITO) substrates [Sanyo, Japan(10 Ω/γ)] were sequentially patterned lithographically; Following this, they were cleaned using detergent, ultrasonicated in deionized water, acetone, and isopropyl alcohol, and dried on a hot plate at 120 °C for 10 min. Then, they were treated using oxygen plasma for 10 min to improve the contact angle just before film coating. The PFF (or PFT or PFSe) film was prepared by using spin-casting MeOH solutions (0.0125 wt%) to form ~10 nm thick films on precleaned ITO glass substrates at 3000 rpm during 30 s in air. The films were then baked at 120 °C for 20 min inside a glove box. For the poly(3,4-ethylene-dioxythiophene):poly(styrene-sulfonate) (PEDOT:PSS, Baytron P 4083 Bayer AG) devices, PEDOT:PSS was passed through a 0.45-mm filter before being deposited onto ITO, at a thickness of ca. 32 nm, via spin-coating at 4000 rpm in air. These films were also dried at 120 °C for 20 min inside a glove box. A blend of $PC_{71}BM$ and PTB7 [1:1.5 (w/w)] in a chlorobenzene/1,8-diiodooctane (97:3, v/v) solution was stirred overnight, filtered through a 0.2 μm poly(tetrafluoroethylene) (PTFE) filter, and then spin-coated (80 nm, 1400 rpm, 30 s) on top of the HTL layer. PFN was subsequently spin cast from a methanol (with acetic acid, 2 μL mL^{-1}) solution with a concentration of 0.5 mg mL^{-1} in air on top of the active layers. The device was completed by depositing thin layers of 100-nm thick aluminum as a cathode at pressures less than 10^{-6} Torr. The active area of the device was 4 mm^2. Finally, the cell was encapsulated using UV-curing glue (Nagase, Japan).

3. Results and discussion

3.1. Synthesis and characterization of polymers

Scheme 1 shows the preparation of a collection of unprecedented p-type CPEs. The resultant copolymers, i.e., PFF, PFT and PFSe, were synthesized via a Stille coupling reaction with M1 and aromatic five-membered heterocyclic compounds (M2 ~ M4: furan, thiophene, and selenophene, respectively). These polymers comprised a conjugated backbone with hydrophilic side chains of sodium butane sulfonates. Upon dissolving the polymers in water/alcohol, a solution with a neutral pH was obtained. The polymers were incorporated as the HTL in polymer:fullerene BHJ solar cells based on a low band-gap donor material, PTB7 (molecular structure shown in Fig. 1) and the $PC_{71}BM$ acceptor, instead of PEDOT:PSS. The p-type CPEs, using different heterocyclic compounds in their backbone, underwent dramatic changes in their dipole strength at the metal anodes/semiconductor interfaces. Extensive

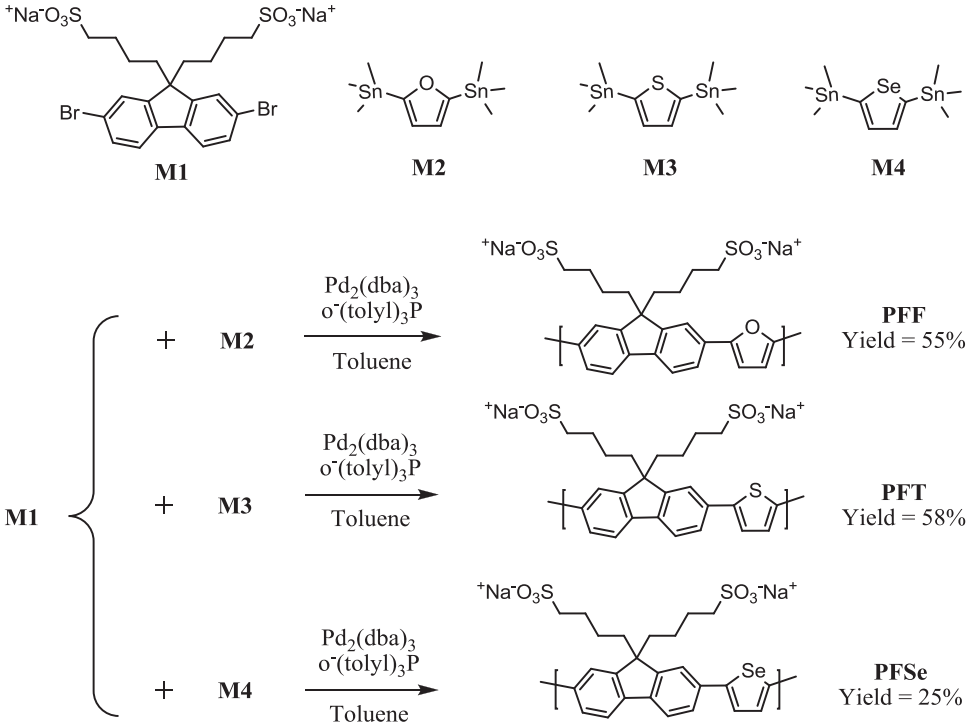

Scheme 1. Synthetic routes of CPE copolymers.

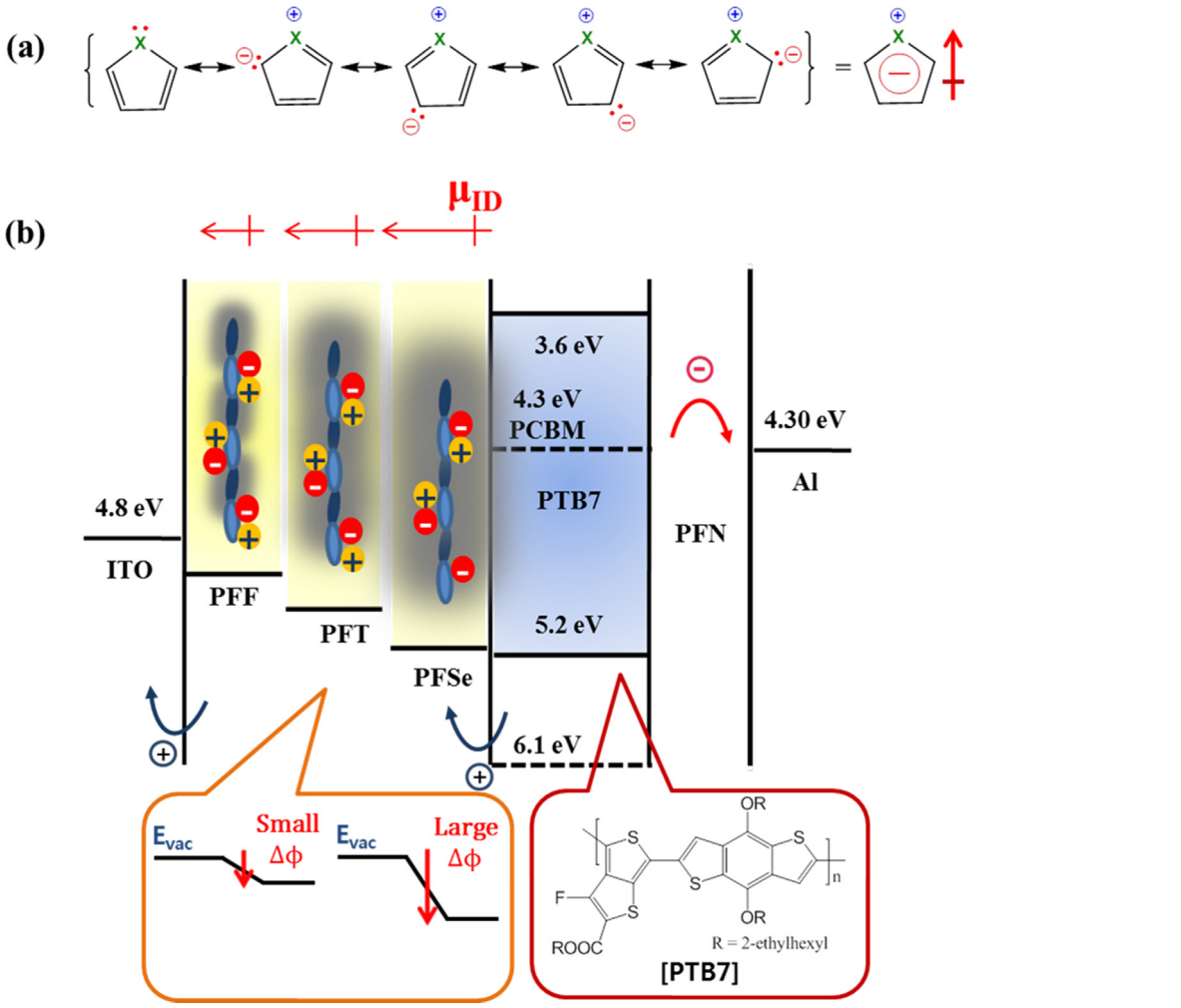

Fig. 1. Schematic illustration of resonance description of heterocyclic rings and its' dipole moment (a), proposed CPEs configurations with varying heterocyclic rings on energy diagram of PSC and their plausible dipole formation (b); sky blue: fluorine, dark blue: heterocyclic ring - π-conjugated backbone, red and yellow: alkyl side chain bearing a sulfonate functional group and sodium ion, respectively. (For interpretation of the references to color in this figure legend, the reader is referred to the web version of this article.)

research has shown that the use of different heterocyclic rings in polymers changes their stability and dipole moment. The aromatic unsaturated compounds, i.e., furan, thiophene and selenophene, have a heteroatom with at least one pair of non-bonding electrons [29,30]. These may combine with the four π-electrons of the double bonds to produce an annulene having an aromatic sextet of electrons. This is illustrated by the resonance description in Fig. 1 (a). The heteroatom (X) becomes sp2-hybridized and develops a positive charge because its electron pair is delocalized around the ring. This delocalization produces a difference in dipole moment compared with the analogous saturated heterocycles, which all have strong dipoles with the heteroatom at the negative end. If atoms of different elements change α values (Slater's exchange parameter), the extra dimension will not only influence the binding characteristics of molecules but also influence the distribution of electrons within the molecules, which has the largest influence on dipole moments [31]. From O to Se, the atomic radius (60→115 pm) of X increases and the electronegativity (3.44→2.55) decreases; however, the dipole moments of the heterocyclic rings, i.e., furan, thiophene and selenophene, still improved because the increase in the atomic radius is larger than the decrease in the electronegativity. Thus, dipole moments of p-type CPEs with heterocyclic rings were expected to increase sequentially (i.e., furan, thiophene and selenophene). Because the stronger dipole moment of CPE makes the vacuum level and the WF of ITO more downshifted, the energy level diagram of materials in PSC devices can be illustrated as in Fig. 1(b).

Table 1
Physical and thermal properties of polymers.

Polymer	Yield [%]	Mn[a] [Da]	Mw[a] [Da]	PDI[a]	T_d [°C]	UV–vis absorption in MeOH solution λ_{max} [nm]
PFF	55	6717	15,248	2.27	442	336
PFT	58	5045	10,980	2.18	438	418
PFSe	25	4383	10,170	2.32	429	420

[a] Determined by GPC in Buffer pH 9+30% MeOH using PEG/PEO to calibrate.

The structures of the copolymers were confirmed via ^{1}H NMR spectroscopy, as shown in Fig. S1 (Supporting information). The ^{1}H NMR spectra of the three materials showed similar features because of the similar polymer backbones. PFF, PFT, and PFSe exhibited excellent solubility in common organic solvents, such as ethanol, methanol, 2-methoxyethanol, DMF, and DMSO. Table 1 summarizes the polymerization results and thermal properties of the copolymers. The weight-average molecular weights (Mw) and polydispersity indexes (PDI) of the copolymers were Mw=15,248 Da with PDI=2.27 for PFF, Mw=10,980 Da with PDI=2.18 for PFT, and Mw=10,170 Da with PDI=2.32 for PFSe,

determined by using gel-permeation chromatography (GPC) using PEG/PEO as the calibration standard, with pH 9 buffer +30% MeOH as the eluent.

The thermal stabilities of the obtained polymers were evaluated using thermogravimetric analysis (TGA); the resulting profiles are presented in Fig. S2. The TGA profiles of all the polymers revealed that 5% of the thermal weight loss in the N_2 environment occurred at a temperature of 429 °C or higher. Thus, all of the synthesized polymers exhibited superior thermal stability, indicative of suitability for device fabrication and application.

3.2. Ultraviolet photoelectron spectroscopy (UPS) analysis

We performed a UPS analysis to investigate the effective WF changes in p-type CPE-covered ITO electrodes when dipole moments of polymers increased. Fig. 2(a) shows UPS spectra of the PFF, PFT, and PFSe layers coated on ITO. UPS spectrum of PEDOT:PSS coated on ITO was also obtained for comparison with the CPEs.

We attained WF values of 4.75, 4.95, and 5.15 eV for PFF, PFT and PFSe, respectively. Specifically, PFSe had a WF 0.15 eV lower than that of PEDOT:PSS (5.0 eV). This value was determined using the equation $WF = h\nu - (E_{cut\text{-}off} - E_F)$, where $h\nu = 21.2$ eV (the incident photon energy for HeI), $E_{cut\text{-}off}$ is at the higher binding energy side (left), and E_F is at the lower binding energy side (right) [32]. $E_{cut\text{-}off}$ corresponds to the vacuum level of the film, which depends on the dipole moment at the interface near the anode. The spontaneous orientation from the ionic group of CPE and its corresponding counter ion forms permanent dipoles at the ITO/active layer interface, and the formation of interfacial dipoles could down-shift the WF of ITO [21]. Based on the UPS result, the energy diagram for BHJ solar cells with the CPEs as the HTL is sketched in Fig. 2(b). By coating CPEs with heterocyclic rings having sequentially stronger dipole moments (i.e., furan→thiophene→selenophene), the secondary cut-off of the CPE-covered ITO electrodes in the range of 17.1–16.7 eV was successively shifted to lower binding energies. This indicates a decrease in the effective WF of the ITO/CPE electrodes. The WF of PFT- and PFSe-coated ITO assures Ohmic contact and satisfactory matching of the energy levels with the HOMO level of the donor material. The surface dipole moments pointing outwards from ITO can reduce the WF of ITO through a downshift to the vacuum level of the active layer. Thus, the energy barrier between the ITO anode and active layer decreases with decreasing work function at the ITO/CPE electrode. This phenomenon facilitates hole extraction from the donor to the ITO side. Conversely, the PFF-coated ITO showed higher WF than pristine ITO; therefore, it worked as an energy barrier between the ITO anode and active layer and interrupted hole transport. For this reason, we predicted that a device using PFF as the HTL will have low Voc and Jsc.

We attribute the gradual decrease in the WF of the synthetic polymer-covered ITO electrodes to the control provided by the different atomic radii of the heteroatoms and thus the dipole moments of the polymers. Facile p-type CPEs that use heterocyclic rings are generated, with the positive pole of the interfacial dipole pointing toward the organic layer and the negative pole toward the ITO, inducing dramatic changes in dipole strength at the anodes/semiconductor interfaces. CPEs composed of π-conjugated backbones with ionic functional groups can reduce the hole-injection barrier between metal anodes and organic active layers in thin-film-based electronic devices. This is essential for those devices that require energy-level-matching at the interface to achieve high performance. This unique property, referred to as WF tunability, results from the formation of an aligned interfacial dipole assembly at the metal/organic semiconductor interface, which modifies the energy-level alignment and improves charge injection [15].

We anticipate that the decreased WFs of the synthetic polymer-covered metal electrodes should allow for efficient collection of the hole carriers when used as anodes in organic solar cells.

3.3. Optical properties

Fig. 3(a) shows the UV–vis absorption spectra of the PFF, PFT and PFSe solutions in methanol. As shown in Table 1, the max absorption bands (λ_{max}) of PFF, PFT and PFSe at 336, 418 and 420 nm correspond to the π–π* transition from the top of the valence band to the bottom of the conduction band [33]. Compared with the absorption spectra of PFF, the absorption spectra of PFT and PFSe are red-shifted by 82 and 84 nm in the solution, respectively. These extensions in the absorption region are attributable to a reduction in the band gap due to the increased electron accepting ability from O to Se. This is because the large

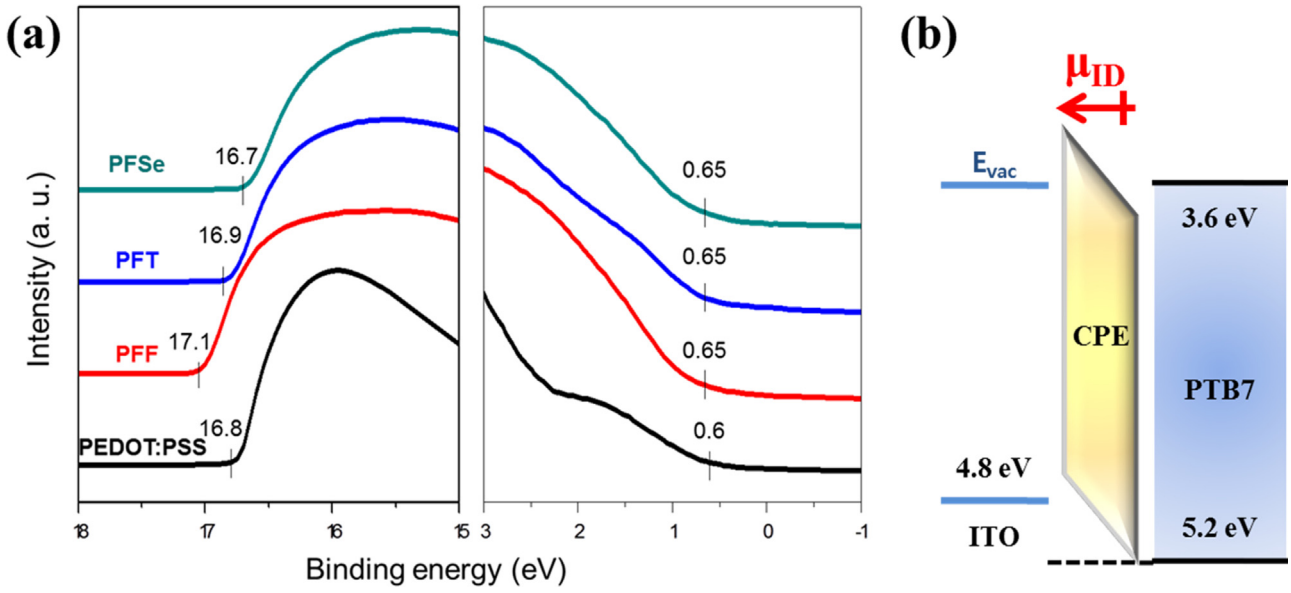

Fig. 2. UPS spectra of the PEDOT:PSS and CPEs (PFF, PFT and PFSe) coated on top of ITO electrodes (a). Interfacial energy diagram of ITO/CPE/PTB7 (b).

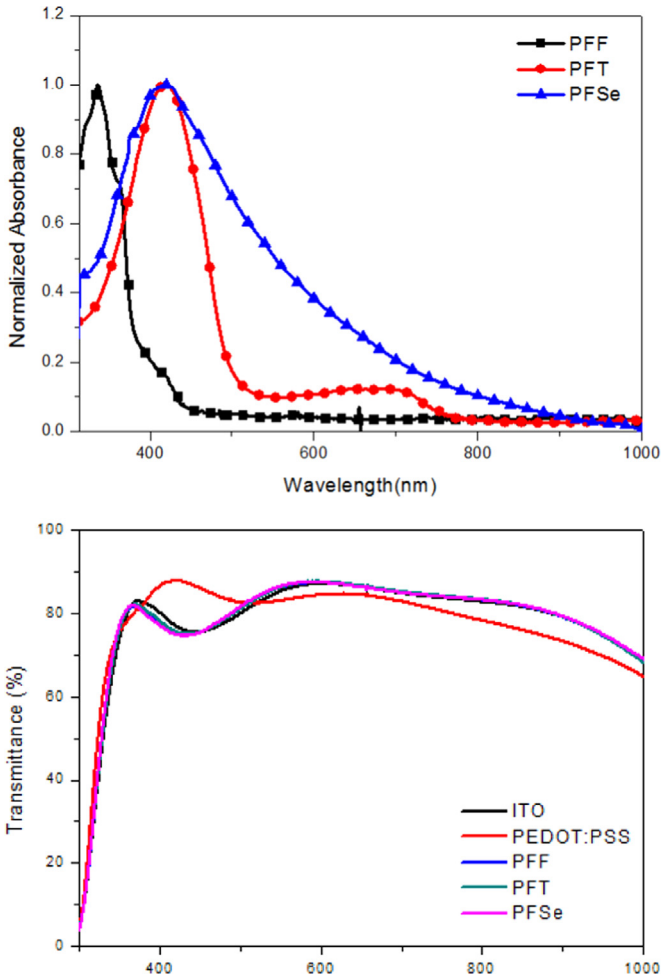

Fig. 3. UV–vis absorption spectra of polymers (PFF, PFT and PFSe) in solution (a) and Comparison of transmittance between PEDOT:PSS and polymers on the ITO substrate (b).

heterocyclic atom provides easier delocalization of the electron clouds along the π-conjugated polymer chains, leading to stronger transition of the conjugated polymer main chain. In other words, the red-shift in UV–vis absorption caused by different heterocyclic atoms is attributed mainly to the lower ionization potential of the larger atom, which leads to a shallow HOMO level and a smaller band gap [34]. The absorption spectra of PFF, PFT and PFSe also indicated that these polymers can absorb only in a narrow optical-wavelength range of the solar spectrum and were suitable HTLs because these polymers can transfer most of the solar flux to the active layer for energy harvesting.

The transmittance spectra of PEDOT:PSS and CPE (PFF, PFT, and PFSe) films spin-coated on ITO substrates are shown in Fig. 3(b). Bare ITO is also included for comparison. Compared with PEDOT:PSS, the films with CPEs showed lower transmittance in the range of 379–500 nm because of their larger bandgap (over 2.4 eV). However, the PFF, PFT, and PFSe films exhibited slightly higher optical densities than PEDOT:PSS in the range of 500–1000 nm because of the low and narrow absorption of CPEs [35]. Regardless of substrates, these CPE films, with a thickness of ~10 nm, exhibited narrow and small light absorption in the visible wavelength region. Therefore, the current density of PSCs using PFF, PFT, and PFSe as a HTL will be higher than that of PEDOT:PSS cells due to the increase of the photon flux of the solar spectrum in the near-IR region.

3.4. Morphological analysis

In conventional solar cells, the surface properties of HTLs deposited on top of the ITO anode can significantly affect the morphology of the active layer, further dictating the light harvesting, exciton dissociation, charge transport and charge collection in organic BHJ solar cells. Investigating the influence of CPEs (PFF, PFT, PFSe) and PEDOT:PSS surface coverage and morphology on PSCs is crucial for determining the resultant performance. To compare the morphology of PEDOT:PSS and CPEs on ITO, AFM was utilized; Fig. 4 presents the topography images. The topographic images of PEDOT:PSS and CPEs surfaces displayed uniform films. Although both PEDOT:PSS and CPEs layers provided uniform films with nanoscale features, we observed an increase in surface roughness of CPEs, with a RMS of 2.67–3.34 nm, compared with the RMS of PEDOT:PSS (1.56 nm). The improved crystallinity and surface roughness of CPEs provides a strong inter-contact at the interface with the PTB7:$PC_{71}BM$ active layer.

The difference in surface potential between the PTB7:$PC_{71}BM$ and HTL films on the ITO was measured via EFM to identify the effective hole extraction properties between the active layer and HTL. The samples were prepared by drop casting a small amount of PTB7:$PC_{71}BM$ blend solution onto the HTL films and then letting it spread slowly while drying to form the interface [36]. The topographic and corresponding surface potential images of polymer:$PC_{71}BM$–HTL are shown in Fig. 5. At the interface of the two layers, the difference in surface potential (ΔSP) of the two distinct parts changed from 59.48 mV to 5.52 mV depending of the type of HTLs. PFF had the largest ΔSP (59.48 mV), while PFSe showed the smallest ΔSP (5.52 mV). This implies that the small potential difference between the active layer and the HTL in the PSC using PFSe as the HTL, facilitated the hole extraction and also increased the probability of dissociation of excitons into free charge carriers, resulting in the improved Voc and Jsc.

3.5. Photovoltaic properties

To verify the merits of CPEs in devices, we fabricated BHJ solar cells using a simple architecture consisting of ITO/HTL (PFF or PFT or PFSe or PEDOT:PSS)/PTB7:$PC_{71}BM$/PFN/Al. The active materials used a solution comprising a blend of PTB7 as a donor and $PC_{71}BM$ as an acceptor (1:1.5 by weight) in a chlorobenzene/1,8-diiodooctane solvent mixture (97:3 by volume). PEDOT:PSS, widely used in solar cells as a HTL, was used to compare the performances of CPEs. The optimal thickness of CPEs as a HTL is found to be approximately 10 nm for 0.0125–0.5 wt% solutions.

Fig. 6(a) presents current density–voltage (J–V) characteristics under AM 1.5 G irradiation (100 $mWcm^{-2}$) of the best PSC performances using PFF or PFT or PFSe or PEDOT:PSS as the HTL. Detailed device parameters are summarized in Table 2. Devices with PEDOT:PSS exhibited a PCE of 6.9%, with a short-circuit current density (J_{SC}) of 13.8 $mAcm^{-2}$, an open-circuit voltage (V_{OC}) of 0.697 V and a fill factor (FF) of 65.7%. In the case of PFF, the PCE was 3.6%, with Jsc of 13.2 $mAcm^2$, Voc of 0.52 V and FF of 49.2%. In the case of PFT, the PCE was 6.5%, with Jsc of 14.3 $mAcm^{-2}$, Voc of 0.64 V and FF of 66.1%. Replacing PEDOT:PSS with PFF and PFT decreased the PCE because of a drop in the Voc. The decrease in Voc can be ascribed to high WF and ΔSP for PFF and PFT (4.75, 4.95 eV and 59.48, 21.28 mV, respectively) when compared to that of PEDOT:PSS (5.0 eV, 20.06 mV). PCE was especially lower in the case of PFF, which also had low Voc and FF due to its limited solubility. However, replacing PEDOT:PSS with PFSe led to a significant enhancement in device efficiency. The device with PFSe yielded a PCE of 7.2%, with J_{SC} of 14.4 $mAcm^{-2}$, V_{OC} of 0.677 V and FF of 69.0%. A simultaneous enhancement of Jsc and FF was observed in the solar cell that used PFSe as a HTL. This enhancement

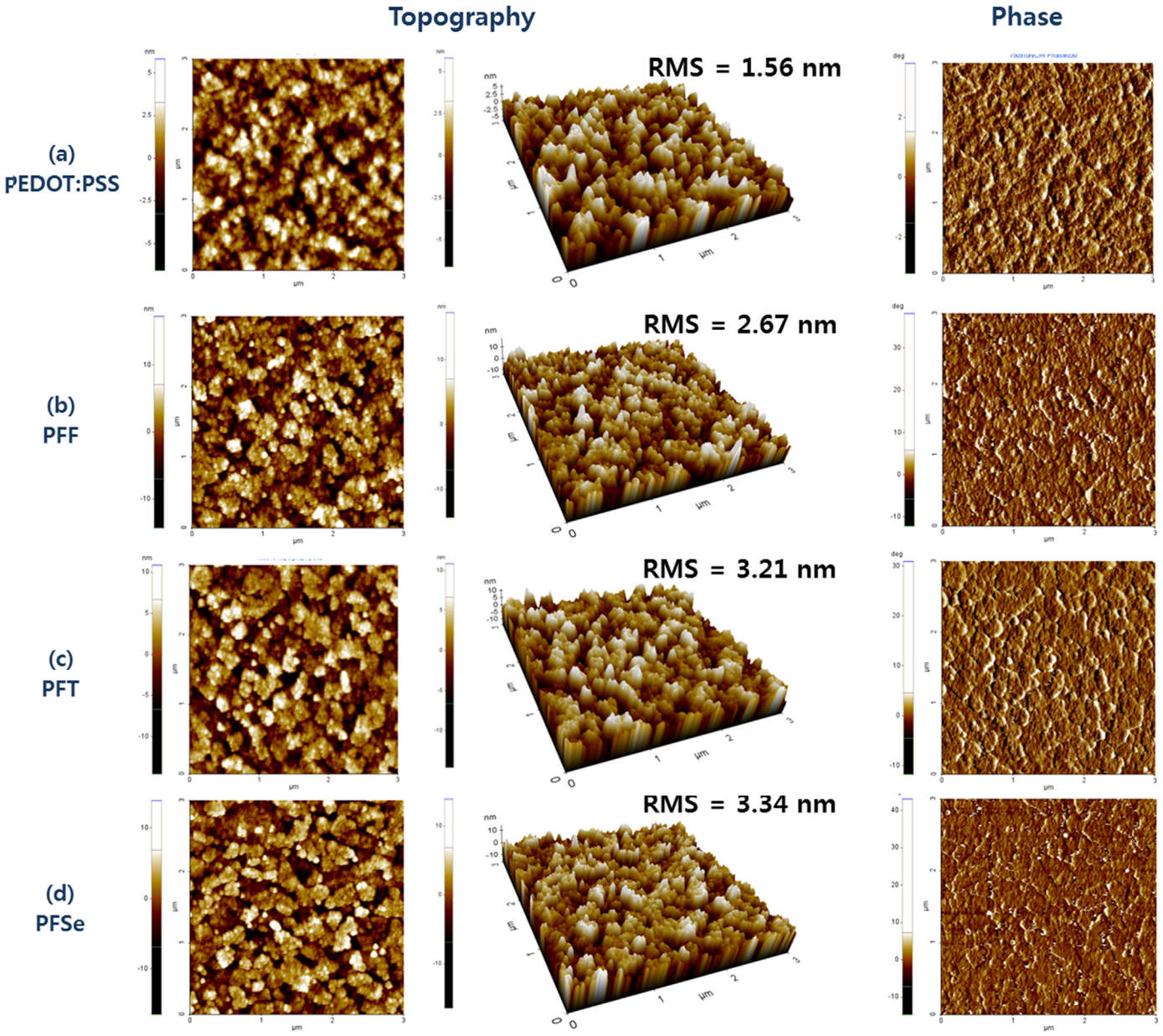

Fig. 4. AFM surface topographic images (size: 3 μm × 3 μm) of PEDOT:PSS (a), CPE layers (b)–(d).

is attributable to the deep WF of the PFSe-covered ITO electrodes, which leads to larger differences in the WF between the ITO/PFSe anode and PFN/Al cathode. This effect induces a larger internal field within the device, leading to efficient sweep-out of photo-generated charge carriers. By increasing the atomic radius of CPE's main chain, dipole moments of the CPE also grow stronger, and the hole extraction and probability of dissociation of excitons also increase due to low ΔSP. ΔSP between the PFSe and active layer is smallest. This finding also indicates that the energy level closely matched that of PTB7. For these reasons, Jsc increased when HTL was changed from PFF to PFSe.

The evolution mentioned above is also reflected in the change of dark curves of the devices (Fig. 6(b)). The device with PFF had high leakage current density in reverse bias and low current density in forward bias, implying poor diode properties. Thus, the solar cell with PFF as a HTL showed lowest Voc and Jsc. The device fabricated with PFT and PFSe showed similar current density in forward bias compared to that of the device made with PEDOT:PSS, but the leakage current was a little lower. Especially, the device with HTL fabricated from PFT had high leakage current and high series resistance compared to that of the device made with PFSe. So Jsc of the device with PFT was lower than PFSe [37].

Fig. 6(c) shows the incident photon conversion efficiency (IPCE) spectra. The EQE spectra of the same devices seemed like the transmittance spectra of the PFF, PFT, PFSe and PEDOT:PSS thin films. Interestingly, the shape of the EQE curve for the device with synthetic polymer HTLs differed from that of the device with PEDOT:PSS. An increase of IPCE at wavelengths in the ranges of 300–480 nm and 550–730 nm was observed for PFF, PFT and PFSe devices in comparison to the PEDOT:PSS control device. This led to a larger Jsc increase from 13.8 mA cm^{-2} to 14.4 mA cm^{-2} under integration. The maximum IPCE in PFSe HTL devices was over 70.8%, indicative of efficient photon-to-electron conversion.

Interestingly, the PCE ($\eta = 7.2\%$) of the PFSe solar cell was higher than that of the device constructed with the widely used PEDOT:PSS HTL ($\eta = 6.9\%$). In Fig. 6(d), we show 480 h of air stability under room temperatures with the PFSe (31.5% decrease) as the HTL. This air stability exhibited an improvement over that with

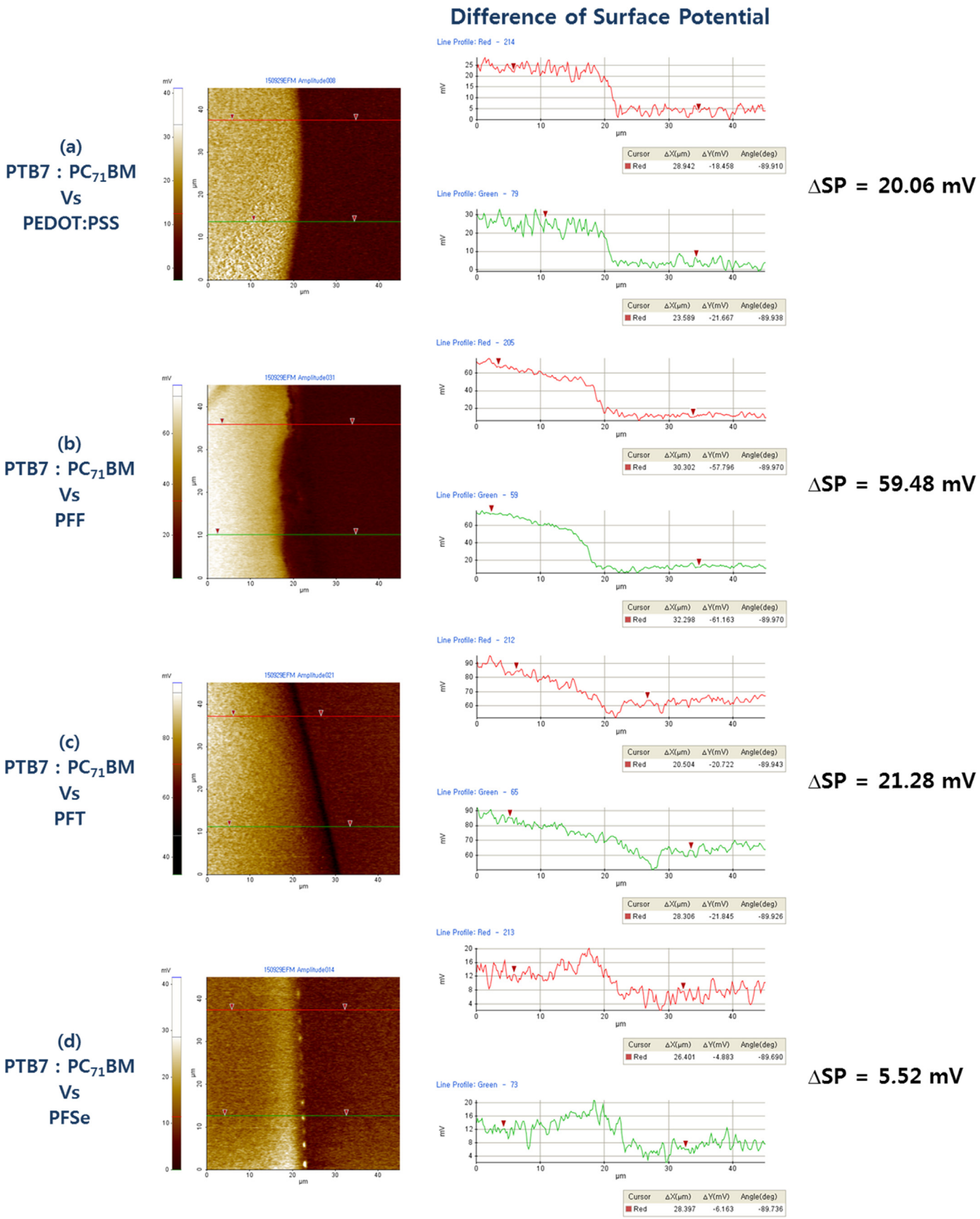

Fig. 5. Surface potential (SP) image of PTB7:$PC_{71}BM$ (left) and CPE (right) and cross-sectional line profile of the SP images: PEDOT:PSS (a), CPE layers (b) ~ (d).

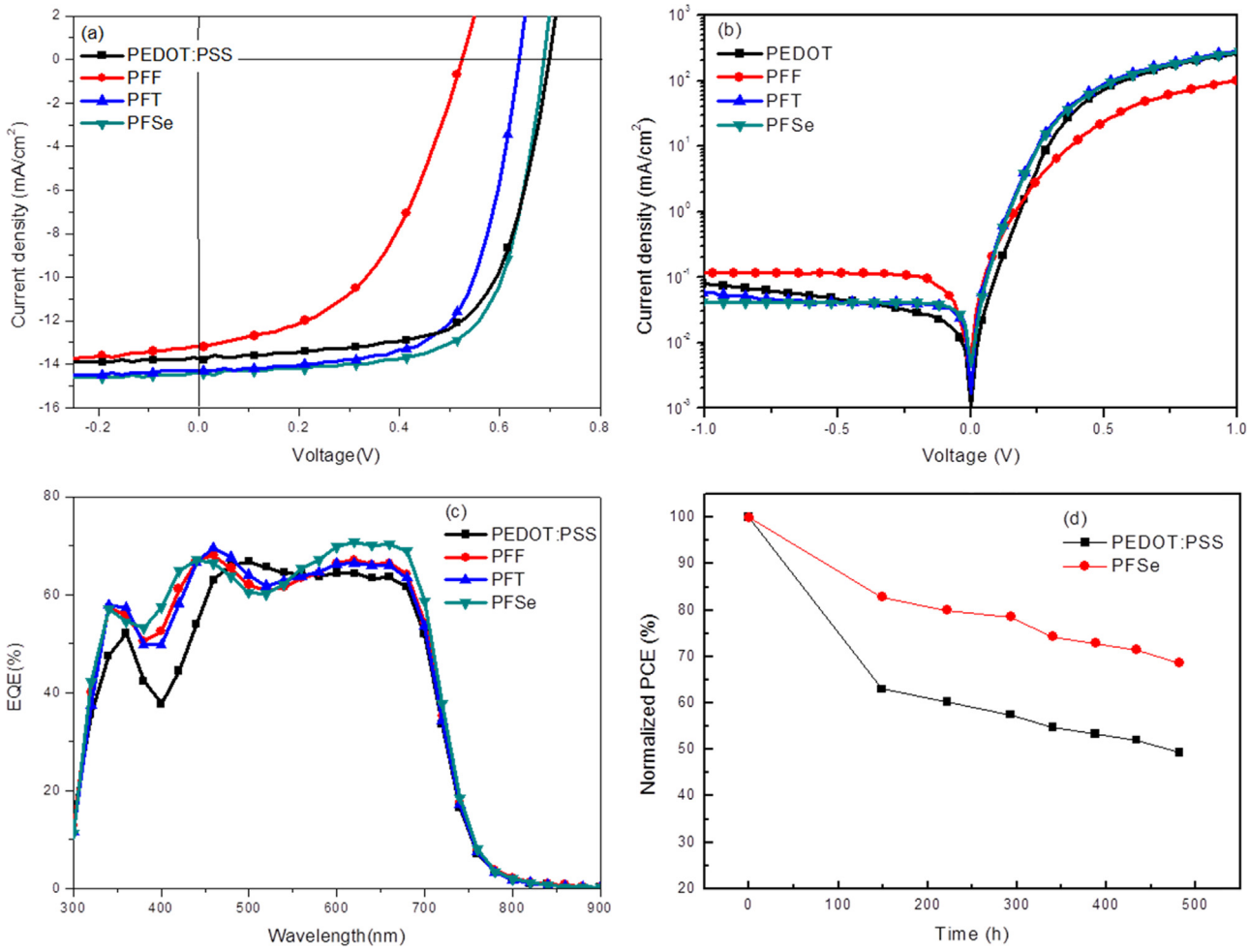

Fig. 6. The J–V curves of the conventional PSC based on PTB7: $PC_{71}BM$ with different HTLs under the illumination of AM 1.5 G, 100 mW/cm^2 (a), dark J–V characteristics (b), EQE spectra of the solar cells (c) and air-stability of the solar cells (d).

Table 2
Photovoltaic properties of the BHJ solar cells using PFF, PFT, PFSe and PEDOT:PSS as HTLs.

HTL	Concentration [wt%]	Jsc [mAcm^{-2}]	Voc [V]	FF [%]	PCE [%]	Rs [Ωcm^2]
PFF	0.0125	13.2	0.515	49.2	3.6	12.61
PFT	0.01	14.3	0.636	66.1	6.5	6.29
PFSe	0.0125	14.4	0.677	69.0	7.2	5.41
PEDOT:PSS	–	13.8	0.697	65.7	6.9	6.80

PEDOT:PSS (50.7% decrease) because of the neutral nature of the synthetic polymer HTLs compared with acidic PEDOT:PSS. The PEDOT:PSS thin film is known to cause device degradation in BHJ solar cells due to its acidic nature [38]; thus, we attribute the extended lifetime of the PFSe solar cell to the neutral pH (6.7–7.0) of the PFSe solution. Notably, we observed improved device lifetimes when using PFSe, which indicates that PFSe can be a promising alternative to PEDOT:PSS as the effective HTL for a PSC.

4. Conclusions

In this study, conductive conjugated polyelectrolytes, i.e., CPEs (PFF, PFT and PFSe), have been successfully incorporated in organic BHJ solar cells as HTLs through solution processing, yielding PCE values of up to 7.2%. PFSe HTL is demonstrated, via a general application in polymer BHJ systems, with the advantage of a strong dipole moment at the interface between the ITO electrode and active layer. Compared with PFF and PFT HTL, an increase in a dipole moment leads to an increase in Jsc and decrease in ΔSP. These results illustrate a novel application of water/alcohol soluble CPEs serving as efficient HTLs for organic BHJ solar cells, which contrasts with the conventionally used HTLs. The device with PFSe as a HTL yielded the best performance (7.2%), with J_{SC} of 14.4 mAcm^{-2}, V_{OC} of 0.677 V and FF of 69.0 %. This device also exhibits an improvement of air stability under room temperature due to the neutral nature.

Notes

The authors declare no competing financial interest.

Acknowledgments

This research was supported by the New & Renewable Energy Core Technology Program of the Korea Institute of Energy Technology Evaluation and Planning (KETEP) grant funded by the Ministry of Trade, industry & Energy (MI, Korea) (No. 20133030000180) and New & Renewable Energy Core Technology Program of the Korea Institute of Energy Technology Evaluation and Planning (KETEP), grant financial resource from the Ministry of Trade, industry & Energy, Republic of Korea (No. 20153010140030).

Appendix A. Supplementary material

Supplementary data associated with this article can be found in the online version at http://dx.doi.org/10.1016/j.solmat.2016.06.017.

References

[1] F.C. Krebs, N. Espinosa, M. Hösel, R.R. Søndergaard, M. Jørgensen, 25th Anniversary article: rise to power – OPV-based solar parks, Adv. Mater. 26 (2014) 29–39.
[2] M.A. Green, K. Emery, Y. Hishikawa, W. Warta, E.D. Dunlop, Solar cell efficiency tables (version 47), Progress. Photovolt.: Res. Appl. 24 (2016) 3–11.
[3] S.-H. Park, S.-J. Lee, J.H. Lee, J. Kal, J. Hahn, H.-K. Kim, Large area roll-to-roll sputtering of transparent ITO/Ag/ITO cathodes for flexible inverted organic solar cell modules, Org. Electron. 30 (2016) 112–121.
[4] P.P. Khlyabich, B. Burkhart, A.E. Rudenko, B.C. Thompson, Optimization and simplification of polymer–fullerene solar cells through polymer and active layer design, Polymer 54 (2013) 5267–5298.
[5] M.-H. Choi, E.J. Ko, Y.W. Han, E.J. Lee, D.K. Moon, Control of polymer-packing orientation in thin films through chemical structure of D-A type polymers and its application in efficient photovoltaic devices, Polymer 74 (2015) 205–215.
[6] K.W. Song, M.H. Choi, H.J. Song, S.W. Heo, J.Y. Lee, D.K. Moon, Effect of replacing proton with alkoxy side chain for donor acceptor type organic photovoltaics, Sol. Energy Mater. Sol. Cells 120 (Part A) (2014) 303–309.
[7] M.A. Uddin, T.H. Lee, S. Xu, S.Y. Park, T. Kim, S. Song, T.L. Nguyen, S.-j Ko, S. Hwang, J.Y. Kim, H.Y. Woo, Interplay of intramolecular noncovalent coulomb interactions for semicrystalline photovoltaic polymers, Chem. Mater. 27 (2015) 5997–6007.
[8] Y. Liu, J. Zhao, Z. Li, C. Mu, W. Ma, H. Hu, K. Jiang, H. Lin, H. Ade, H. Yan, Aggregation and morphology control enables multiple cases of high-efficiency polymer solar cells, Nat. Commun. 5 (2014) 5293.
[9] Y. Liang, Z. Xu, J. Xia, S.-T. Tsai, Y. Wu, G. Li, C. Ray, L. Yu, For the bright future—bulk heterojunction polymer solar cells with power conversion efficiency of 7.4%, Adv. Mater. 22 (2010) E135–E138.
[10] S.-H. Liao, H.-J. Jhuo, Y.-S. Cheng, S.-A. Chen, Fullerene derivative-doped zinc oxide nanofilm as the cathode of inverted polymer solar cells with low-bandgap polymer (PTB7-Th) for high performance, Adv. Mater. 25 (2013) 4766–4771.
[11] K. Zhang, Z. Hu, R. Xu, X.-F. Jiang, H.-L. Yip, F. Huang, Y. Cao, High-performance polymer solar cells with electrostatic layer-by-layer self-assembled conjugated polyelectrolytes as the cathode interlayer, Adv. Mater. 27 (2015) 3607–3613.
[12] L. Lu, W. Chen, T. Xu, L. Yu, High-performance ternary blend polymer solar cells involving both energy transfer and hole relay processes, Nat. Commun. 6 (2015) 7327.
[13] E.J. Lee, S.W. Heo, Y.W. Han, D.K Moon, An organic-inorganic hybrid interlayer for improved electron extraction in inverted polymer solar cells, J. Mater. Chem. C (2016), doi:10.1039c1035tc03754a.
[14] H.F. Dam, N.P. Holmes, T.R. Andersen, T.T. Larsen-Olsen, M. Barr, A.L. D. Kilcoyne, X. Zhou, P.C. Dastoor, F.C. Krebs, W.J. Belcher, The effect of mesomorphology upon the performance of nanoparticulate organic photovoltaic devices, Sol. Energy Mater. Sol. Cells 138 (2015) 102–108.
[15] H. Zhou, Y. Zhang, C.-K. Mai, S.D. Collins, T.-Q. Nguyen, G.C. Bazan, A.J. Heeger, Conductive conjugated polyelectrolyte as hole-transporting layer for organic bulk heterojunction solar cells, Adv. Mater. 26 (2014) 780–785.
[16] M.T. Lloyd, C.H. Peters, A. Garcia, I.V. Kauvar, J.J. Berry, M.O. Reese, M. D. McGehee, D.S. Ginley, D.C. Olson, Influence of the hole-transport layer on the initial behavior and lifetime of inverted organic photovoltaics, Sol. Energy Mater. Sol. Cells 95 (2011) 1382–1388.
[17] C.E. Petoukhoff, D.K. Vijapurapu, D.M. O'Carroll, Computational comparison of conventional and inverted organic photovoltaic performance parameters with varying metal electrode surface workfunction, Solar Energy Materials and Solar Cells 120 (Part B) (2014) 572–583.
[18] M. Li, W. Ni, B. Kan, X. Wan, L. Zhang, Q. Zhang, G. Long, Y. Zuo, Y. Chen, Graphene quantum dots as the hole transport layer material for high-performance organic solar cells, Phys. Chem. Chem. Phys. 15 (2013) 18973–18978.
[19] E. Bovill, N. Scarratt, J. Griffin, H. Yi, A. Iraqi, A.R. Buckley, J.W. Kingsley, D. G. Lidzey, The role of the hole-extraction layer in determining the operational stability of a polycarbazole: fullerene bulk-heterojunction photovoltaic device, Appl. Phys. Lett. 106 (2015) 073301.
[20] P.F. Ndione, A. Garcia, N.E. Widjonarko, A.K. Sigdel, K.X. Steirer, D.C. Olson, P. A. Parilla, D.S. Ginley, N.R. Armstong, R.E. Richards, E.L. Ratcliff, J.J. Berry, Highly-tunable nickel cobalt oxide as a low-temperature P-type contact in organic photovoltaic devices, Adv. Energy Mater. 3 (2013) 524–531.
[21] L. Chen, C. Xie, Y. Chen, Influences of charge of conjugated polymer electrolytes cathode interlayer for bulk-heterojunction polymer solar cells, Org. Electron. 14 (2013) 1551–1561.
[22] W. Xu, X. Zhang, Q. Hu, L. Zhao, X. Teng, W.-Y. Lai, R. Xia, J. Nelson, W. Huang, D.D.C. Bradley, Fluorene-based cathode interlayer polymers for high performance solution processed organic optoelectronic devices, Org. Electron. 15 (2014) 1244–1253.
[23] H.I. Kim, T.T.T. Bui, G.-W. Kim, G. Kang, W.S. Shin, T. Park, A. Benzodithiophene-Based Novel, Electron transport layer for a highly efficient polymer solar cell, ACS Appl. Mater. Interfaces 6 (2014) 15875–15880.
[24] Z. He, C. Zhong, S. Su, M. Xu, H. Wu, Y. Cao, Enhanced power-conversion efficiency in polymer solar cells using an inverted device structure, Nat. Photon. 6 (2012) 591–595.
[25] T.T. Do, H.S. Hong, Y.E. Ha, J. Park, Y.-C. Kang, J.H. Kim, Effect of polyelectrolyte electron collection layer counteranion on the properties of polymer solar cells, ACS Appl. Mater. Interfaces 7 (2015) 3335–3341.
[26] B.H. Lee, J.-H. Lee, S.Y. Jeong, S.B. Park, S.H. Lee, K. Lee, Broad work-function tunability of p-type conjugated polyelectrolytes for efficient organic solar cells, Adv. Energy Mater. 5 (2015) 1401653.
[27] K.E. Laidig, P. Speers, A. Streitwieser, Origin of depressed dipole moments in five-membered, unsaturated heterocycles, Can. J. Chem. 74 (1996) 1215–1220.
[28] C. Duan, K. Zhang, C. Zhong, F. Huang, Y. Cao, Recent advances in water/alcohol-soluble [small pi]-conjugated materials: new materials and growing applications in solar cells, Chem. Soc. Rev. 42 (2013) 9071–9104.
[29] B.M. Wong, J.G. Cordaro, Electronic properties of vinylene-linked heterocyclic conducting polymers: predictive design and rational guidance from DFT calculations, J. Phys. Chem. C 115 (2011) 18333–18341.
[30] Y. Li, J.B. Lagowski, Electric field effects on bipolaron transport in heterocyclic conjugated polymers with application to polythiophene, Opt. Mater. 32 (2010) 1177–1187.
[31] B.I. Dunlap, S.P. Karna, R.R. Zope, Dipole moments from atomic-number-dependent potentials in analytic density-functional theory, J. Chem. Phys. 125 (2006) 214104.
[32] H. Zhou, Y. Zhang, C.-K. Mai, J. Seifter, T.-Q. Nguyen, G.C. Bazan, A.J. Heeger, Solution-processed pH-neutral conjugated polyelectrolyte improves interfacial contact in organic solar cells, ACS Nano 9 (2015) 371–377.
[33] D.-M. Kim, K.-B. Shim, J.I. Son, S.S. Reddy, Y.-B. Shim, Spectroelectrochemical and electrochromic behaviors of newly synthesized poly[3′-(2-aminopyrimidyl)-2,2′:5′,2″-terthiophene], Electrochimica Acta 104 (2013) 322–329.
[34] S. Das, P.B. Pati, S.S. Zade, Cyclopenta[c]thiophene-based D–A conjugated copolymers: effect of heteroatoms (S, Se, and N) of benzazole acceptors on the properties of polymers, Macromolecules 45 (2012) 5410–5417.
[35] H. Choi, C.-K. Mai, H.-B. Kim, J. Jeong, S. Song, G.C. Bazan, J.Y. Kim, A.J. Heeger, Conjugated polyelectrolyte hole transport layer for inverted-type perovskite solar cells, Nat. Commun. 6 (2015) 7348.
[36] Y. Zhu, Z. Yuan, W. Cui, Z. Wu, Q. Sun, S. Wang, Z. Kang, B. Sun, A cost-effective commercial soluble oxide cluster for highly efficient and stable organic solar cells, J. Mater. Chem. A 2 (2014) 1436–1442.
[37] W. Qiu, R. Müller, E. Voroshazi, B. Conings, R. Carleer, H.-G. Boyen, M. Turbiez, L. Froyen, P. Heremans, A. Hadipour, Nafion-modified MoOx as effective room-temperature hole injection layer for stable, high-performance inverted organic solar cells, ACS Appl. Mater. Interfaces 7 (2015) 3581–3589.
[38] B. Ecker, J.C. Nolasco, J. Pallarés, L.F. Marsal, J. Posdorfer, J. Parisi, E. von Hauff, Degradation effects related to the hole transport layer in organic solar cells, Adv. Funct. Mater. 21 (2011) 2705–2711.